The Hyperbolic Chemical Bond: Fourier Analysis of Ground and First Excited State Potential Energy Curves of HX (X = H−Ne)

John A. Harrison*

Institute of Fundamental Sciences, Massey University, Private Bag 102-904 NSMSC, Auckland, New Zealand

Received: November 20, 2007; Revised Manuscript Received: June 24, 2008

RHF/aug-cc-pV*n*Z, UHF/aug-cc-pV*n*Z, and QCISD/aug-cc-pV*n*Z, $n = 2-5$, potential energy curves of H_2 X $^1\Sigma_g^+$ are analyzed by Fourier transform methods after transformation to a new coordinate system via an inverse hyperbolic cosine coordinate mapping. The Fourier frequency domain spectra are interpreted in terms of underlying mathematical behavior giving rise to distinctive features. There is a clear difference between the underlying mathematical nature of the potential energy curves calculated at the HF and full-CI levels. The method is particularly suited to the analysis of potential energy curves obtained at the highest levels of theory because the Fourier spectra are observed to be of a compact nature, with the envelope of the Fourier frequency coefficients decaying in magnitude in an exponential manner. The finite number of Fourier coefficients required to describe the CI curves allows for an optimum sampling strategy to be developed, corresponding to that required for exponential and geometric convergence. The underlying random numerical noise due to the finite convergence criterion is also a clearly identifiable feature in the Fourier spectrum. The methodology is applied to the analysis of MRCI potential energy curves for the ground and first excited states of HX (X = H−Ne). All potential energy curves exhibit structure in the Fourier spectrum consistent with the existence of resonances. The compact nature of the Fourier spectra following the inverse hyperbolic cosine coordinate mapping is highly suggestive that there is some advantage in viewing the chemical bond as having an underlying hyperbolic nature.

Introduction

Fourier analysis is particularly advantageous for physical situations where the Fourier spectrum is relatively compact compared to the data it describes. In the cases where the features in the Fourier spectrum are interpretable, great insight into the physical phenomena being studied can often be obtained.[1] Analysis of the Fourier spectrum allows one to make decisions regarding the nature of the spacing of the data points (i.e., sampling frequency) required to achieve a certain numerical accuracy via the well-known Nyquist−Shannon sampling theorem.[2,3] In addition, Fourier expansion allows the application of interpolation and noise filtering techniques in a well-defined and computationally efficient manner through application of the fast Fourier transform. The ease with which first and higher derivatives can be obtained by inverse transformation following multiplication in the frequency domain facilitates topological analysis of curves and surfaces. Another significant advantage for the analysis of multidimensional systems is the straightforward generalization to higher dimensionality that the Fourier- and other related transform-based methods possess.

Fourier analysis is not a routine tool in the analysis of molecular potential energy surfaces. An example of why this is the case is clearly shown by Figure 1 which presents the H_2 ground-state potential energy curve between 0.20 and 5.32 Å and the corresponding Fourier transform. In general, an equal number of Fourier frequency components are required to accurately describe the original data. The reason originates from the need to have both high frequencies to describe the steep repulsive part at small R_{H-H} of the potential and low frequencies for the shallow, attractive part at large internuclear separation. From Figure 1, the absolute magnitude of the Fourier components can be seen to decay with increasing frequency. At high frequencies, n, this decay exhibits an approximate $n^{-2.0}$ dependence, indicative of a function with an impulsive second derivative. The absence of oscillatory behavior in the decay region indicates that the point at which the second derivative is impulsive is located at the origin. The Fourier spectrum is thus neither more compact nor more informative than the original potential energy curve, and there is nothing to be gained in performing it. This, in itself, is not an unusual observation for a physical system when spatial frequencies are considered and is characteristic of a nonlinear relationship between the coordinate and the potential function relating to it. If a method could be found to minimize the number of Fourier components required to describe the molecular potential energy curve, via a simple coordinate transformation, application of Fourier-transform-based techniques could be of immediate use for application in molecular dynamics studies where it is essential to have an efficient sampling methodology because of the expense of performing large numbers of high-quality calculations.

The question of minimization of the number of Fourier components is related to the nature of the convergence of a function when expressed as a series of basis functions. Although an expansion in a Fourier series is not the only option and may not be the most rapidly converging choice, the methodology of Fourier analysis is well established and represents a general starting point. Boyd[4] distinguishes between algebraic and exponential convergence of series expansions. Algebraic convergence is characterized by the algebraic index of convergence, k, where k is the largest number for which

* E-mail: j.a.harrison@massey.ac.nz.

10.1021/jp804945z CCC: $40.75
Published on Web 08/13/2008

$$\lim_{n\to\infty} |a_n| n^k < \infty \qquad n \gg 1 \tag{1}$$

where a_n are the coefficients of the series.

When the coefficients, a_n, decrease faster than $1/n^k$, for any finite value of k, the series exhibits exponential (or infinite-order) convergence. Exponential convergence is required for any optimal spectral decomposition algorithm. Analysis of the rate of convergence is complicated by the requirement that it is the behavior at large n which is indicative of the nature of the convergence. In evaluating the nature of the convergence, it is the supremum limit that is required, and this can be difficult to establish where there are many oscillatory, interfering components present. The exponential index of convergence r is obtained from the following expression,

$$r = \lim_{n\to\infty} \frac{\ln|\ln|a_n||}{\ln(n)} \tag{2}$$

so that (equivalently),

$$a_n \approx s e^{-q} \qquad {}^{n^r}n \gg 1,\ s \text{ and } q \text{ are constants} \tag{3}$$

Furthermore, it is necessary to distinguish between supergeometric, geometric, and subgeometric convergence depending on value of the limit.

$$\lim_{n\to\infty} \frac{\ln|a_n|}{n} \tag{4}$$

Where this limit tends to infinity, the series is said to have supergeometric convergence; it has geometric convergence if it tends to a constant and subgeometric convergence if it tends to zero. The significance of this classification scheme relates to the underlying mathematical nature of the function. Of particular relevance to this work is that functions that have exponential and geometric convergence are indicative of those with singularities (e.g., poles) in the complex plane. The exponential rate of decay of the transformed spectrum is limited at high frequencies by the singularity located nearest to the real axis. The rate of decay is related to the position of the singularity by

$$F(z) = F(x + iy)$$

and if the Fourier series only converges within the strip, $|y| < \rho$, (x arbitrary),

$$\lim_{n\to\infty} |a_n / a_{n+1}| = e^{\rho} \tag{5}$$

A pole or other singularity located on the real axis leads to subgeometric or algebraic convergence.

Recently, the notion of smoothness has been applied as a criterion for the evaluation of the quality of calculated potential energy curves. The distinction has been made between chemical and mathematical smoothness. Head-Gordon et al.[5,6] have developed lccsd methods to calculate smooth curves by applying a bumping algorithm. In these studies, mathematical smoothness was used to describe the continuity of the potential energy curve itself, as well as first and second derivatives, whereas the idea of chemical smoothness is related to the introduction of artificial maxima, minima, and points of inflection by the computational methodology. These concepts are naturally related to the question of the location of singularities and of the contribution of noise (and the origin of that noise) on the curve and are most easily treated if a harmonic analysis can be performed on the curve in question. Random (white) noise affecting all points of the curve will have a Fourier spectrum with an intensity that is flat with no obvious periodic features. An example of this is the limit in numerical convergence, where often energies are converged to, for example, 10^{-7} a.u., and therefore, smaller place values will have random numerical values. Noise due to the existence of a discontinuous derivative of nth order will appear as a decay, with an algebraic order of convergence relating to the order for which the derivative becomes impulsive. Furthermore, the decay will exhibit oscillations with the period of oscillation relating to the position of the discontinuity (via the shift theorem). In order to formalize the application of these concepts, it is necessary to perform some form of harmonic analysis to quantify both the nature and magnitude of the convergence limiting features and noise present. However, because there is an inherent singularity at the point where the position of the two nuclei coincide (where the nuclear repulsion energy becomes infinite), such analysis cannot be applied to the potential function in the usual internuclear coordinate system. If Fourier analysis is applied, the Fourier coefficients are doomed to decay algebraically with an algebraic index of convergence equal to two, as the spectrum in Figure 1 illustrates. A way of avoiding this catastrophe is to map the potential to a coordinate system which places this point far enough off the real axis that it will not limit the convergence rate of the Fourier series at high frequencies. A mapping utilizing a hyperbolic-coordinate transformation would seem to be ideally suited to achieving this goal.

Because current computational chemical methods cannot calculate the form of the whole potential curve simultaneously but are limited to sampling points along it, there is also the implicit assumption that this sampling occurs at sufficiently close intervals (typically 0.001 Å) so that no chemical information is lost. There has so far, however, not been any systematic attempt at formalizing what functional form this chemical information

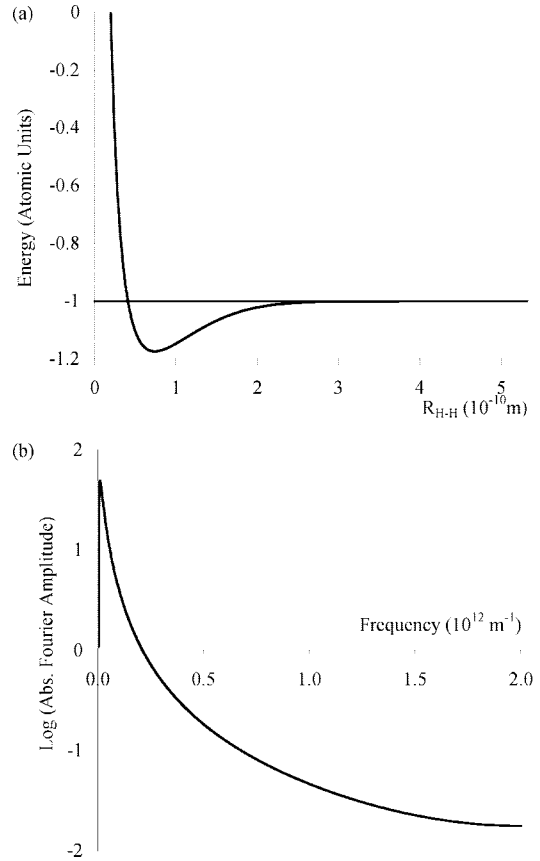

Figure 1. (a) QCISD/aug-cc-pV5Z potential energy curve and (b) the corresponding Fourier frequency spectrum.

might take, nor what optimum sampling methodology is required to capture it to any predetermined accuracy.

This paper is organized in two sections. Because this is the first attempt at utilizing this type of analysis, the first section details a study on the H_2 ground-state system as a prototypical example of the range of numerical applications that the approach has. In particular, the nature of the potential energy curves calculated at HF and full-CI levels are compared as well as the influence of the size of basis set. The second section details a comparison between the Fourier-transformed curves for the set of ground and first excited multiconfiguration reference internally contracted configuration interaction (MRCI) calculated potential curves of the molecules HX (X = H−Ne) to establish the nature of the information that can be extracted from the transformed curves.

Computational Details

The coordinate transformation given by eq 6, which was obtained by trial and error, has been used in this study in an heuristic attempt to find a solution to the problem of obtaining a compact representation in Fourier space.

$$\cosh(a\eta) = k\left(R_{\text{H-H}} - R_0 + \frac{1}{k}\right) \tag{6}$$

The assumption upon which this coordinate transformation is based is that the potential energy curve in question has hyperbolic character with respect to the internuclear distance, $R_{\text{H−H}}$. Although a hyperbolic relationship has never been associated with the underlying nature of the chemical bond, it is a relationship that has been useful in the analysis of other physical systems, and it becomes of fundamental interest to examine the effects following the change in coordinate system represented by eq 6. The values of the constants used in the preliminary study of the ground state of hydrogen are $a = 4$, $R_0 = 0.21725$ Å, and $k = 8.6537$ Å^{-1}. Values of η ranging from 0 to 2 were sampled, corresponding to internuclear separations, $R_{\text{H−H}}$, of 0.21725−170.9968 Å. The value of R_0 was chosen to give a curve which has approximately unit height (in a.u.) for all levels of theory. It should be stressed that these values, obtained by trial and error, do not carry any obvious physical significance, because no theory currently exists for the prediction of these values from any established physical principles. No attempt was therefore made to assign any physical significance to the (spatial) frequency scale. The value for the factor a, in the coordinate transformation, is arbitrary, resulting only in a convenient range of 0−2 for the η coordinate.

A total of 1024 evenly spaced (with respect to η) points was calculated at the UHF, RHF, and full-CI level (via a QCISD calculation) with each of the basis sets[7−11] aug-cc-pVnZ (n = 2−5) by using Gaussian98.[12] Convergence failure for RHF and QCISD methods occurred for five distances at (the same) large values of $R_{\text{H−H}}$ (<5.1 Å), and in these cases, it was necessary to interpolate from adjacent points. For these five points, the error introduced by this procedure is estimated to be of the same order of magnitude as the convergence criterion for the energy of 10^{-8} a.u. Although the QCISD calculations give, in principle, the same values as the full-CI results obtained by other algorithms, minor differences in the stability of the algorithm at large $R_{\text{H−H}}$ had significant impacts on the noise floor in the Fourier spectrum. Therefore, in such a case, the particular method of calculation may become significant. Fourier transforms were obtained by performing a fast Fourier transform on a double-sided data set in order to obtain a symmetric transform that has no imaginary (sine) component. Because no frequency scale has been imposed on the transformed data, the frequency components referred to in this part of the study are the 2048 spatial frequency components obtained from transformation of the 2048 point double-sided data sets.

The ground and first excited states of HX (X = H−Ne) were calculated by using a slightly modified version of the above procedure with different constants. Because the observed transforms are only weakly dependent on small variations of the constants in eq 6, the R_0 for each curve was chosen to coincide with the zero in the total calculated energy rather than the arbitrary value of 1 a.u. above the minimum of the potential curve for the preliminary study. Revised values of k (12.245522 Å^{-1}) and a (3.9539) were used, giving a range of η from 0 to 2 for R_{XH} of R_0 to around 110 Å. With the exception of H_2 (where Gaussian98 was employed), all potential curves were calculated by using 512 evenly spaced (with respect to η) points over the range R_0−110 Å (approximately) by using the MRCI algorithm of MOLPRO[13−15] following an initial MCSCF[16,17] calculation at each point. These data sets were augmented to 2048 points by padding with the asymptotic energy value before Fourier transforming the double-sided curve (containing 4096 points). Padding in this fashion has the effect of interpolation in the transformed domain, yielding curves which are visually easier to interpret but not containing any additional information.

Results and Discussion

1. Application to H_2 X $^1\Sigma_g^+$. *HF Results.* The RHF and UHF curves in the transformed coordinate η are given in Figures 2a and 3a, respectively. The RHF and UHF curves for each basis set are numerically identical up to the point $R_{\text{H−H}} = 1.217$ Å whereupon they diverge. The corresponding Fourier spectra are given in Figures 2b−d and 3b−d. The point at which the RHF and UHF divergence occurs is evident in the Fourier-transform spectrum of the UHF data set where it manifests itself as oscillations, the period of which relates to the point where the discontinuity occurs. Analysis of the amplitude of the modulated component in the Fourier spectrum of the UHF/aug-cc-pV5Z curve for large values of the frequency yields an $n^{-3.00\pm0.05}$ algebraic dependence. Such dependence is definitive evidence for an impulsive third derivative (i.e., discontinuous second derivative) of the original function. The points of discontinuity, which correspond to the onset of spin contamination in the UHF wave functions and concomitant change to exponential decay (see below) at large R, for each of the basis sets, are given in Table 1 (obtained from the G98 calculations), and these are in agreement with those obtained from the Fourier spectra.

Taking the difference between $V(R_{\text{H−H}})$ and the calculated energy of two hydrogen atoms, for the portion of the UHF curve after the point of discontinuity, yields an exponential decay with respect to $R_{\text{H−H}}$ (Figure 4). The decays were fit to eq 7

$$V(\infty) - V(R_{\text{H-H}}) = Ae^{-B(R_{\text{H-H}} - R^{\text{d}}_{\text{H-H}})} \tag{7}$$

where $R^{\text{d}}_{\text{H−H}}$ is the internuclear distance at which point the UHF and RHF curves diverge. The fitted constants for eq 7 are given in Table 2. From Figure 4, the exponential relationship can be seen to hold over a greater range of internuclear distance as the size of the basis set is increased. For the aug-cc-pV5Z basis set, the exponential relationship extends beyond five orders of magnitude of $V(\infty) - V(R_{\text{H−H}})$ with only a 0.7% average relative deviation from exponential behavior.

In the case of the RHF potential curves, no large discontinuity is observed as indicated by the absence of significant oscillations in the Fourier spectrum. Small oscillations are evident with a

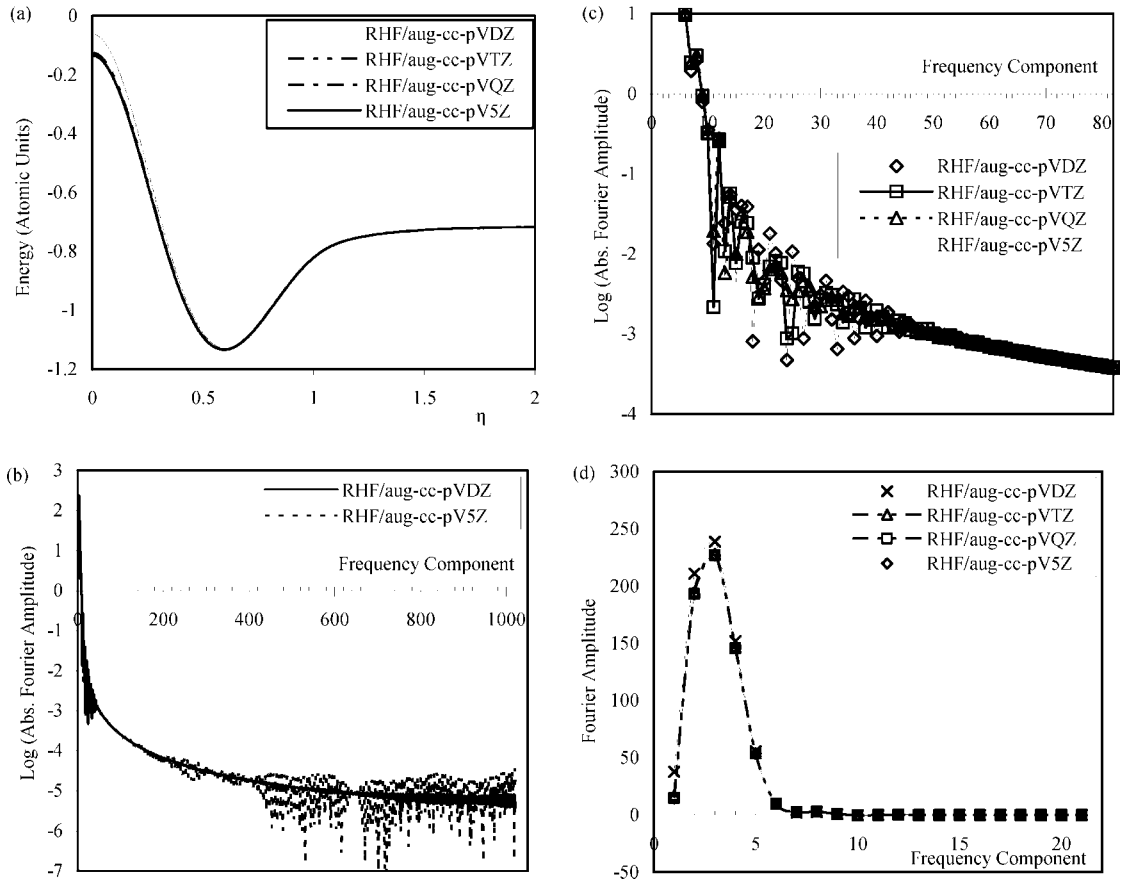

Figure 2. Transformed RHF potentials and their Fourier spectra. (a) RHF curves in the η coordinate system. (b) Full-frequency spectra (absolute values plotted). Aug-cc-pVTZ and aug-cc-pVQZ spectra are similar to the aug-cc-pVDZ spectrum and are omitted for clarity. (c) Mid-frequency region (absolute values plotted). (d) Low-frequency region.

frequency corresponding to the truncation at the last point calculated (at 170.9968 Å), in agreement with the observation that even at this distance, the RHF curves have not converged to their limiting values. The oscillations evident in the aug-cc-pV5Z high-frequency region of the Fourier spectrum originate from numerical instabilities at large R, which were observed only for this basis set. If the RHF potential curves are referenced to the value of the potential at infinite separation (for practical purposes, this was calculated at an internuclear separation of 5×10^9 Å), the potential decays proportionately to $R_{H-H}^{-1.001 \pm 0.005}$ for distances greater than 7.5 Å. Equivalently, as is expected for correspondingly large values of η (where the function cosh approximates to a single exponential term), the potential decays exponentially with respect to η with the decay constant close to 4 (actual value for the RHF/aug-cc-pV5Z curve: 3.9888). The Fourier spectrum for the RHF/aug-cc-pV5Z curve exhibits algebraic $n^{-1.98 \pm 0.04}$ dependence for the decay at high frequency, indicating that the second derivative of the potential curve is impulsive. This is expected because of the cusp generated at the mid point of the data set when the double-sided data set is generated, because the curve has not yet reached its asymptotic value, even at 171 Å, and therefore has a discontinuous first derivative. In this case, the algebraic index of convergence, $k = 2$, arises as a consequence of the finite sampling window used rather than being due to any inherent property of the potential energy curve.

QCISD Results. The transformed QCISD potential energy curves are given in Figure 5a. At large R_{H-H}, the potential should decay with an expected R_{H-H}^{-6} dependence, consistent with induced-dipole−induced-dipole interaction between the atoms. Correspondingly, in the η coordinate system, the decay should appear exponential with a limiting decay constant of −24, and this is indeed the case for $R_{H-H} > 6$ Å ($\eta > 1.16$), where the constants for the QCISD/aug-cc-pVDZ, TZ, QZ, and 5Z curves are −23.96, −24.32, −24.61, and −24.60, respectively.

The Fourier spectra of the QCISD potential energy curves are shown in Figure 5b−d. Three distinct regions are identifiable in the Fourier spectrum. Most of the intensity occurs for the low frequencies, as is expected. The second portion contains an approximately exponential decay of an oscillatory component, and the third region represents the noise floor.

The existence of an exponentially decaying oscillatory component in the frequency spectrum is evidence that the original potential energy curve (in the η coordinate system) has continuous derivatives to all orders. With reference to the shift theorem, oscillations in the frequency spectrum indicate that there is some underlying change in behavior originating at the point related to the frequency of oscillations. The exponential convergence noted for the mid-frequency region of the Fourier spectrum is characteristic of a singularity lying on the complex plane, located off the real axis. Physically, this type of mathematical structure is usually associated with resonant behavior. The fundamental difference in the case presented here, from the usual application of the term, is that the resonance is of a spatial nature; that is, it is centered about a particular value of the mapped coordinate, η, rather than a particular value for the energy (or equivalently, the frequency corresponding to the energy). In addition, the exponential decay constant obtained from the spatial Fourier frequency spectrum presented in this analysis relates to the spatial width of the underlying feature contributing to the potential rather than the width of a spectral feature with respect to the energy coordinate. This is a demonstration that although solutions to the time-independent Schrödinger

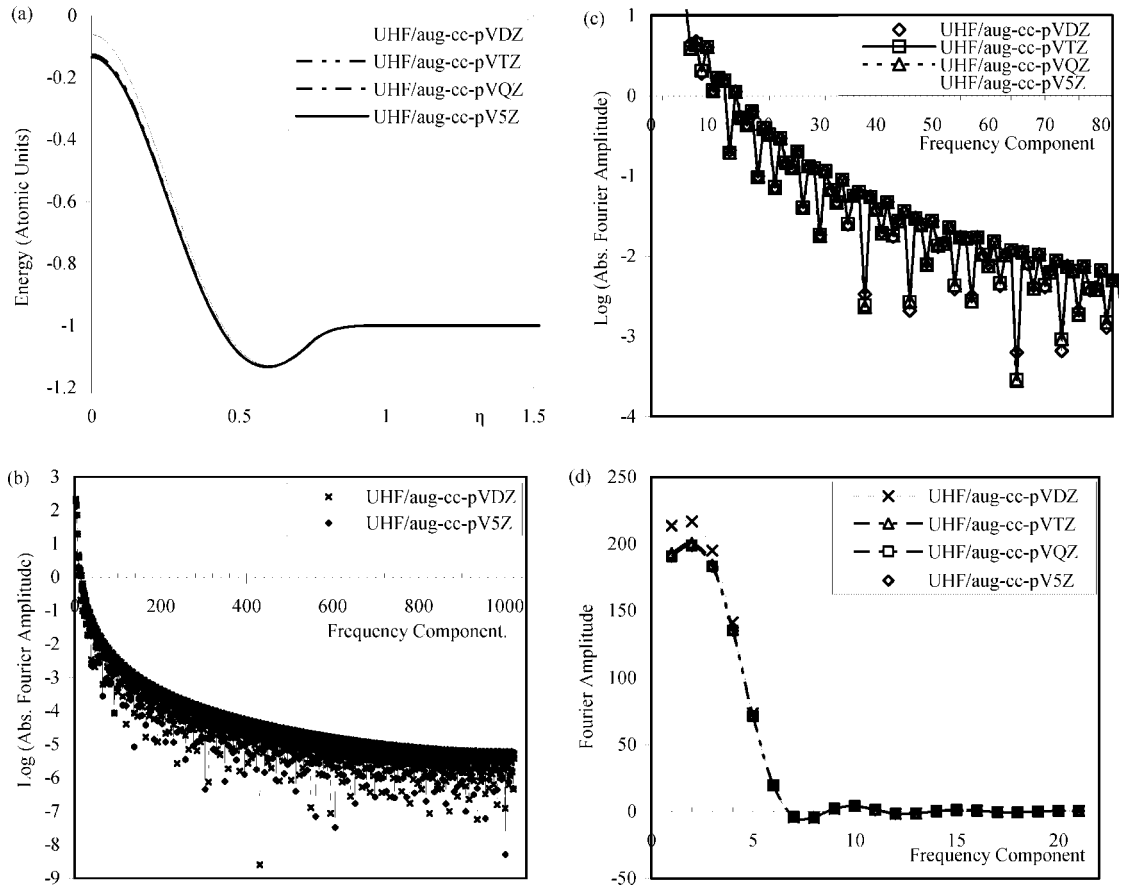

Figure 3. Transformed UHF potentials and their Fourier spectra. (a) UHF curves in the η coordinate system. (b) Full-frequency spectra (absolute values plotted). Aug-cc-pVTZ and aug-cc-pVQZ spectra are similar to the aug-cc-pV5Z spectrum and are omitted for clarity. (c) Mid-frequency region (absolute values plotted). (d) Low-frequency region.

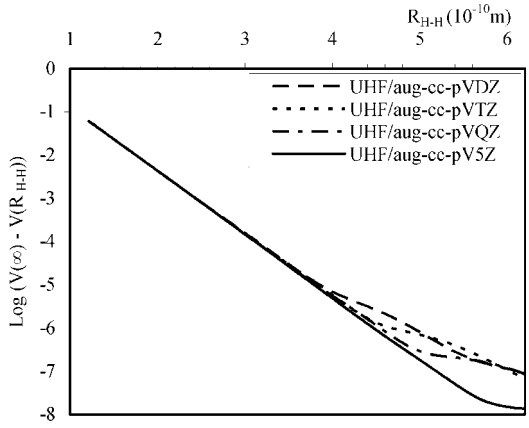

Figure 4. Exponential decay of the UHF potential curves in the region following the RHF/UHF bifurcation point.

TABLE 1: Location of the RHF/UHF Bifurcation Point (Onset of Spin Contamination in the UHF Wavefunction)

basis set	R_{H-H} bifurcation (Å)	η	energy (a.u.)
aug-cc-pVDZ	1.21966	0.73999	−1.0579719
aug-cc-pVTZ	1.21660	0.73930	−1.0596936
aug-cc-pVQZ	1.21660	0.73930	−1.0599789
aug-cc-pV5Z	1.21655	0.73929	−1.0600727

equation are of a stationary nature (with respect to energy), nonstationary behavior with respect to spatial coordinates will still be evident. The mathematical nature of this nonstationary behavior with respect to the coordinate corresponding to the internuclear distance takes on a particularly transparent form following the hyperbolic coordinate mapping. Given that the coordinate point about which the resonance is centered seems to be associated with a switch from the limiting induced-dipole−induced-dipole interaction to the onset of electron correlation, as shown in Figure 6, it is tempting to associate the position of this resonance with the usual chemical notion of a transition state, although the use of the term for this situation requires further refinement (see below). Because the derivatives to all orders are continuous (neglecting the white numerical noise), the transition from one regime to the other is not a discontinuous one but rather perfectly smooth.

TABLE 2: Analysis of the Exponential Decay Region of The UHF Potential Curves Shown in Figure 4[a]

dasis set	maximum R_{H-H} (Å)	A (a.u.)	B (Å)$^{-1}$	R^2
aug-cc-pVDZ	3.184	−0.0593568	3.34532	0.999965
aug-cc-pVTZ	3.184	−0.0600103	3.36408	0.999999
aug-cc-pVQZ	3.705	−0.0600973	3.36770	0.999999
aug-cc-pV5Z	4.482	−0.0607021	3.38425	0.999994

[a] Data between the bifurcation points listed in Table 1 and the maximum value given were used. R is the least-squares correlation coefficient for the fit of the log values plotted in Figure 4.

The decay region varies only slightly between basis sets with only the DZ curve showing a difference in the frequency. Isolating the exponential decay region and applying eq 8,

$$C^{\cdot}(\xi) = C(\xi)\frac{\xi}{e^{-0.2353\xi}} \tag{8}$$

(where ξ is the frequency) and normalizing the amplitudes yields the oscillatory components shown in Figure 7. As can be seen from the figure, the oscillatory component is well approximated

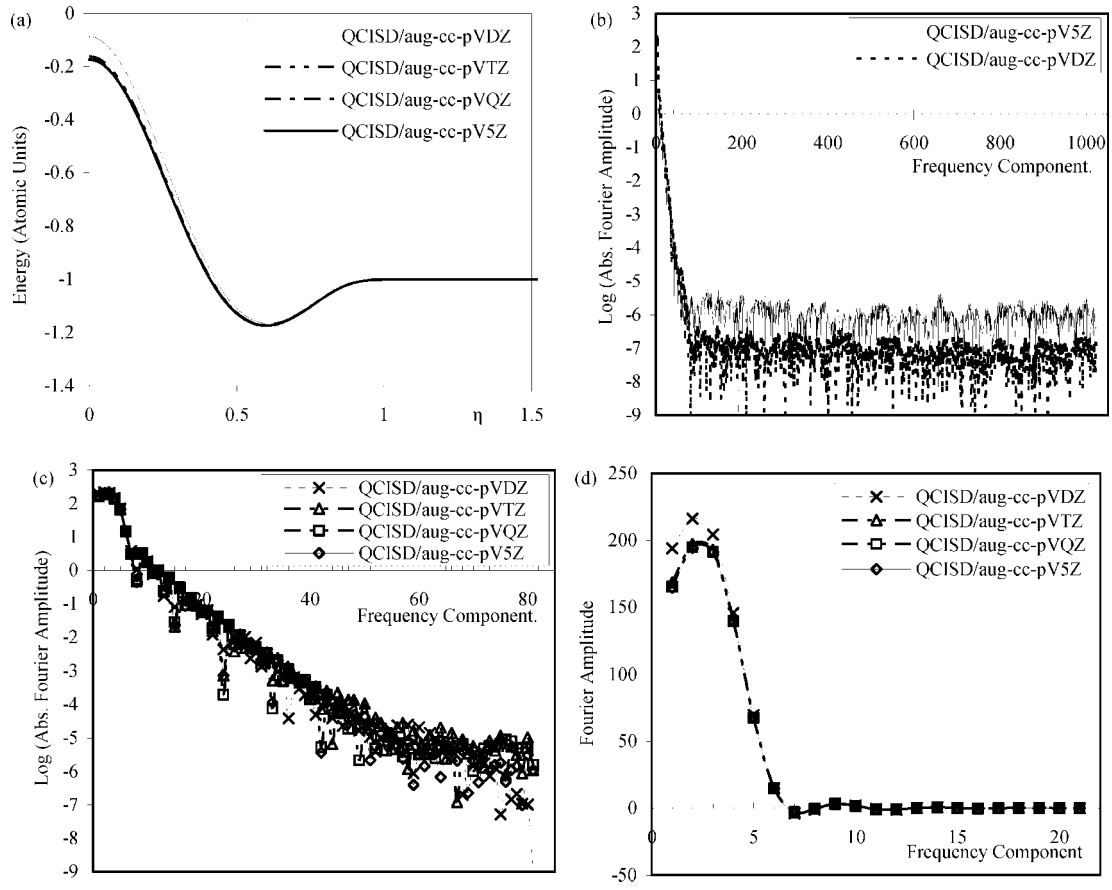

Figure 5. Transformed QCISD potentials and their Fourier spectra. (a) QCISD curves in the η coordinate system. (b) Full-frequency spectra (absolute values plotted). Aug-cc-pVTZ and aug-cc-pVQZ spectra are similar to the aug-cc-pV5Z spectrum and are omitted for clarity. (c) Mid-frequency exponential decay region (absolute values plotted). (d) Low-frequency region.

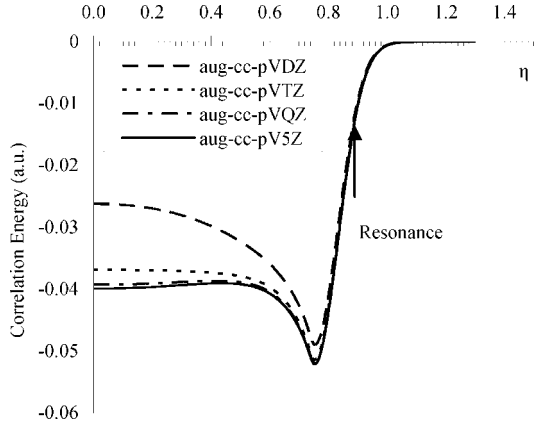

Figure 6. Correlation energy in the η coordinate system. The curves represent the QCISD(η)−UHF(η) values.

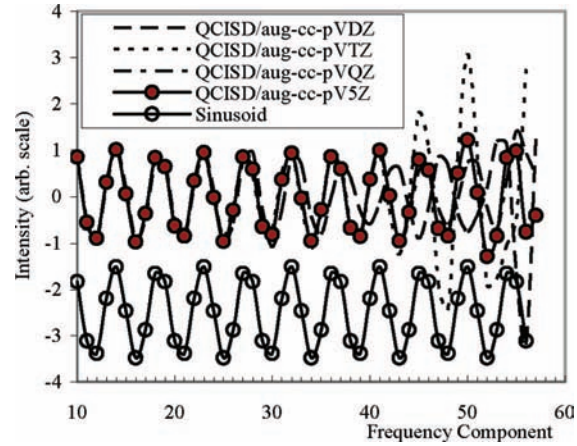

Figure 7. The portion of the exponential decay region weighted to remove the frequency and exponential terms. The sinusoid in the lower portion of the graph has been offset by 2.5 units and has been sampled and smoothed in a fashion identical to that for the QCISD curves for comparative purposes.

by the single sine-wave component shown. At low frequency, all the oscillations for each of the basis sets are in phase with each other. At higher frequencies, the oscillations become dephased, and the magnitudes of the oscillations are no longer regular. It is clear that the smaller basis sets exhibit this behavior at frequencies lower than those of the larger basis sets, and therefore, the limiting behavior for an infinite basis set appears to be that represented by the single-sinusoidal component in Figure 7. Analysis of the frequency of the oscillations indicates a corresponding position of 1.6866 Å ($\eta = 0.8276$) for the DZ curve and 2.1260 Å ($\eta = 0.88889$) for the three largest basis sets. Interestingly, this latter value lies close to the value of four times the Bohr radius ($4a_0 = 2.1167$ Å).

The ultimate noise level in the frequency spectra would be expected to be of the order of 10^{-8} a.u. (consistent with the convergence criterion), but as is evident from the log plot, Figure 5b, the readily identifiable noise level is one order of magnitude larger for the aug-cc-pVDZ basis set and two orders of magnitude for the larger basis sets. The cause of this appears to be minor instabilities at $R_{H-H} > 4$ Å which are readily observed if the second derivative (with respect to η) of the potential energy curve is examined. It is therefore possible to introduce a high-frequency cutoff by examination of the

TABLE 3: Determination of the Minimum Energy Point (Equilibrium Bond Length) from Interpolation of the Derivative Curve for Various Sampling Regimes[a]

number of sampling points	minimum from interpolation (Å)	interpolating function	number of points used for interpolation	R^2 (for interpolating function)
8	0.876649	linear	2	(1)
16	0.744637	cubic	4	(1)
32	0.741739	cubic	4	(1)
64	0.741651	cubic	7	0.99999972
128	0.741620	cubic	12	0.99999997
256	0.741622	cubic	17	0.99999997
512	0.741621	cubic	32	0.99999997
1024	0.741619	cubic	65	0.99999997

[a] The optimum sampling corresponds to 64 points with oversampling occurring for 128−1024 points and undersampling occurring for 8−32 points.

magnitude of the Fourier components. Using a practical criterion for the introduction of this cutoff as the ratio of the absolute value of the Fourier coefficient to the rms noise value equal to four yields a cutoff at the 60th frequency component (not counting the zero frequency value). By setting the values of the frequency components higher than this to zero for the QCISD/aug-cc-pV5Z potential curve and comparing the inverse transform to the original curve, it is found that there is no significant difference (root-mean-square difference $= 1.3\ 10^{-8}$ a.u.; maximum deviation $= 3.5\ 10^{-7}$ a.u. over the entire 1024 points of the original potential energy curve, as expected). The most important consequence of this observation is that the same information would be obtained if the potential curve had been sampled by using only 60 (corresponding to twice the highest frequency) evenly spaced points over the same range of coordinate η rather than the 1024 points used in this study. For practical purposes, 64 points are required in order to utilize the numerical advantages of using the fast Fourier transform algorithm which requires the length of the data set to be a power of 2. This translates to a 16-fold saving in computational time for this potential energy curve for all basis sets at the QCISD level. Furthermore, because the curve needs only to be calculated to the point at which the energy is within 10^{-7} a.u. (i.e., within the observed noise level) of the asymptotic dissociation limit, the actual number of points needing computation is reduced to around two-thirds of this value, corresponding to values of R_{H-H} less than 15 Å. This is a minor saving compared to the removal of oversampling because the relative computational expense of points for very large values of R_{H-H} is small. At the UHF and RHF level, no such saving is possible because the components of the Fourier spectra do not converge to the underlying noise level in the exponential manner that the QCISD values do, nor, in the RHF case, do the values of the potential converge to the asymptotic value at the maximum bond length used in this study (i.e., up to 171 Å).

Oversampling can have beneficial effects if the noise originates from random sources. By oversampling and averaging over n points, the precision of each of the Fourier components improves with dependence proportional to the square root of the number of samples. This may be used as a strategy to improve the accuracy of the highest frequency Fourier coefficients which possess a low signal-to-noise ratio. The very slight change in the calculated minimum energy point accompanying oversampling is given in Table 3 and corresponds to fitting the background noise. If the function is undersampled, a corresponding error will be introduced, equivalent to the intensity of the components which have been lost by truncation in the frequency domain.

It could be argued that the nuclear−nuclear repulsion energy term should be subtracted from the total energy before the analysis is applied to avoid the singularity associated with $R = 0$ and yielding a smooth function more amenable to Fourier analysis. The effect of removing this term is straightforward to ascertain because the Fourier transform is a linear transformation, and terms remain additive in the transformed domain. At the origin of the mapped coordinate system, the mapping reduces to an exponential relationship, and hence, any function that is increasing at a less than exponential rate (i.e., functions with algebraic rate of increase) will be mapped to a function that has a gradient of zero at the new coordinate system origin. The H_2 nuclear−nuclear repulsion term calculated for the nuclear distances used in the coordinate system of Part 2 (below) is shown in Figure 8a, and the absolute values of the corresponding Fourier coefficients are shown in Figure 8b. The effect of the hyperbolic mapping (Figure 8c) to the new coordinate system is to place the singularity arising from the nuclear−nuclear repulsion far enough from the real axis that it does not limit the rate of convergence of the Fourier series at high frequency. As can be seen in Figure 8b, this is indeed the case because the Fourier series of the nuclear−nuclear repulsion energy in the transformed coordinate system converges much more rapidly than the corresponding convergence for the total H_2 potential. Any observations and conclusions drawn from analysis of the high-frequency region apply equally to both the total energy as well as the electronic energy. The limiting behavior for the coefficients of the ground state in Figure 8b must be established by renumbering the coefficients after all redundancies have been removed. This effectively removes all interpolation and the effects of double-siding the spectrum, so that an optimum sampling is used, with only the minimum number of points chosen. The limiting behaviors for the coefficients after applying the new numbering scheme, n', are shown in Figure 9a,b for eqs 2 and 4, respectively. Only the values corresponding to integral numbers of n' are necessary; however, the nonintegral values have been retained in the plots to give a clearer view of the supremum limits. From the figures, it can be seen that for the region corresponding to exponential convergence, r tends to the value 1.0 (Figure 9a), and the limit for eq 4 is a constant (Figure 9b). This is sufficient to establish the exponential and geometric nature of the Fourier-series convergence. The limiting rate of exponential convergence can hence be attributed to singularities lying elsewhere on the complex plane. The RHF and UHF curves both demonstrate algebraic convergence indicating that these levels of theory place the position of the convergence limiting singularity on the real axis. The QCISD curve has the limiting singularity located off the real axis as

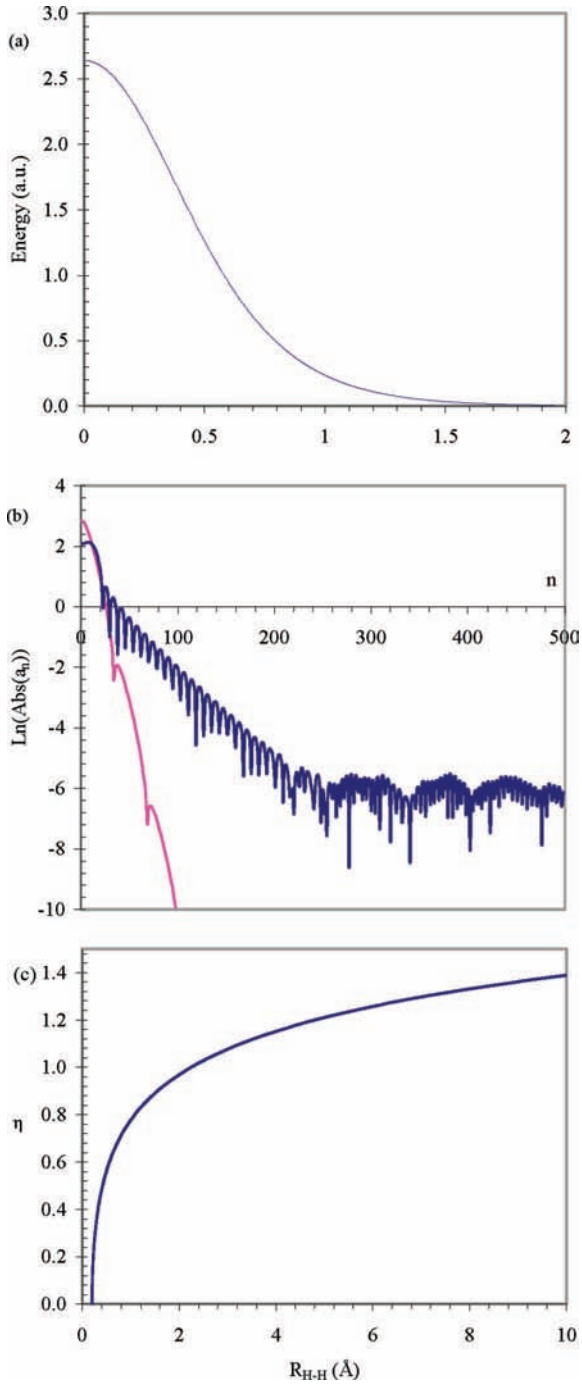

Figure 8. Nuclear−nuclear repulsion energy term for the ground state of H_2 following inverse cosh mapping (a) and the corresponding Fourier amplitudes (b). The upper curve in panel b is the corresponding Fourier amplitude plot for the total energy. (c) Relationship between the internuclear distance R_{H-H} (<10 Å) and the mapped coordinate system η.

exponential convergence is clearly evident in the frequency region up to the region where the high-frequency white-noise floor (attributable to finite numerical precision) dominates.

Analysis of the Stationary Points in the Potential Energy Curve. An additional application is the identification of the stationary points of the potential energy curve. In particular, the minimum energy point corresponding to the equilibrium nuclear configuration has special significance to chemistry. This point may be readily identified by calculating the first derivative and obtaining the zero-crossing points. The first derivative is most easily obtained by applying the derivative theorem, eq 9,

$$\int_{-\infty}^{\infty} V'(\eta) e^{-i2\pi\eta\xi}\, d\eta = i2\pi\xi F(\xi) \qquad (9)$$

(where $F(\xi)$ is the Fourier transform of $V(\eta)$) and applying the inverse transform. The second derivative is as easily obtained by a second application of the theorem before applying the inverse transform. The minimum point is then obtained by interpolating the first derivative in the region of the minimum and solving the interpolating function.

It is instructive to illustrate the corresponding accuracy by which the minimum of the curve can be established by the above procedure as a function of the sampling interval. Table 3 details the accuracy obtained from the various sampling strategies. The curve was resampled, and the Fourier transform was obtained. The derivative was calculated by applying eq 9. Points around the zero crossing were fit to a cubic expression (with the exception of the eight-point sample which was fit with a linear interpolating function), which was then solved. Application of the inverse of the coordinate transformation then gives the minimum of the curve in the normal R_{H-H} coordinate system as given in Table 3. The table clearly shows a steep dependence on the number of points used if undersampling is employed (8−64 points) and minimal change in the oversampling region (64−1024 points). The error in the undersampling regime is compounded by the inadequacies of the fitting function because of the small number of points to fit, as well as the error introduced by truncation in the frequency domain. The data

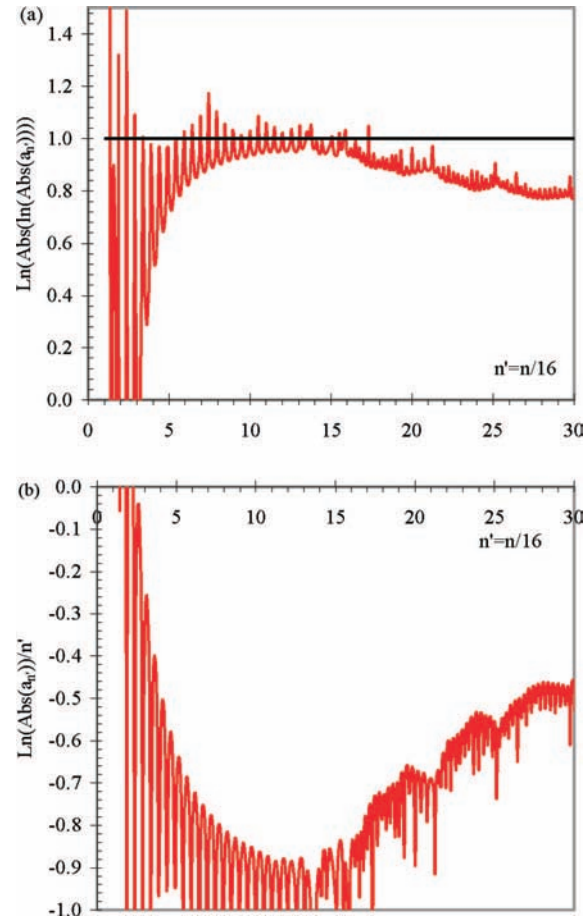

Figure 9. (a) Limiting behavior for Fourier coefficients. The asymptotic behavior for the lower bound tends toward 1 for the coefficients $n' <$ 13, indicating exponential convergence (exponential index of convergence, $r = 1$). Above $n' = 13$, algebraic convergence is evident. (b) The trend to a (upper) limit evident around $n' = 13$ indicates geometric convergence.

TABLE 4: Comparison of Extrapolated Fourier Coefficients[a]

freq. coeff.	aug-cc-pVDZ	aug-cc-pVTZ	aug-cc-pVQZ	aug-cc-pV5Z	extrapolated	R^2
0	−1866.0087	−1896.1276	−1900.3057	−1901.1341	−1901.6121	0.99999
1	194.0795	168.6371	165.3397	164.7823	164.2325	0.99990
2	216.1317	197.3216	194.8859	194.5150	194.0825	0.99986
3	204.3253	193.0285	191.5093	191.3205	191.0538	0.99987
4	145.8061	140.4421	139.5953	139.5173	139.4148	0.99974
5	69.4731	67.7449	67.3143	67.2854	67.2941	0.99414

[a] The R value is the correlation coefficient obtained from the linear least-squares fit used for the extrapolation.

TABLE 5: Computational Parameters for the Calculated Equilibrium Bond Length R_{H-H} and Dissociation Energy, D_e

method	equilibrium R_{H-H} (Å)	D_e (a.u.)
QCISD/aug-cc-pV5Z	0.74162	0.1742627
zero frequency extrapolation	0.74162	0.1744858
six term extrapolation	0.74112	0.1743441
MRCI/aug-cc-pV6Z [20]	0.74154	0.1743609
exact	0.74143[a]	0.1744757[b]

[a] Experimental value from ref 19. [b] Born−Oppenheimer value from ref 18.

presented in Table 3 further serve to illustrate that it is not necessary to directly calculate the energy at the position of the minimum as long as an adequate strategy has been employed to adequately determine the frequency components that simultaneously describe the whole of the curve.

Extrapolation to the Infinite Basis Set Limit. A linear dependence between the value of a particular Fourier coefficient and $1/N^2$, where N is the number of basis functions, was noted for the low-frequency region. This relationship was noted to hold only for those components that were sufficiently far away from the highest gradient regions in the Fourier frequency spectrum. Because the frequency spectrum is dominated by only a few components at low frequency, significant improvement can be gained by extrapolating only these components. For the QCISD results, this corresponds to the lowest six frequencies (inclusive of the zero-frequency value). The six lowest frequency Fourier components and their extrapolated values are listed in Table 4, along with the correlation coefficients of the least-squares fits. For a symmetric data set of 2048 data points, a change in amplitude in the frequency spectrum of 1 unit for a single component will result in a change in amplitude of that sinusoidal component by an amount of 2/2048 or approximately 10^{-3} a.u when the inverse transform is taken. The zero-frequency peak contributes 1/2048 (and represents a shift of the whole curve up or down) and has the greatest effect. If corrections are applied to the six lowest frequencies (with the remainder of the frequencies obtained from the QCISD/aug-cc-pV5Z being retained without further correction), an improvement to the parameters for the minimum energy region is obtained. These are compared in Table 5. The value for the minimum energy from extrapolation of only the zero-frequency values shows surprisingly good agreement with the most accurate available value within the Born−Oppenheimer approximation,[18] the error being only 10 μhartree (or 2.2 cm^{-1}).

The $1/N^2$ dependence noted for the convergence with respect to the number of basis functions demonstrates that the convergence with respect to the number of basis functions is algebraic and hence far from optimal (i.e., exponential). The reason for this is discussed by Boyd[4] and has its origins in the need to relate the choice of basis functions to a chemically sensible starting point for the calculation.

2. Application to HX (X = H−Ne) Ground and First Excited States. The set of states comprising the ground and first excited electronic states of HX, where X = H−Ne, includes states of various symmetries and spin multiplicities, states arising from avoided crossings and states of a repulsive nature, while also being small enough to be accessible to high levels of theory. The following molecular states were examined: H_2 X $^1\Sigma_g^+$ and b $^3\Sigma_u^+$; HeH, X $^2\Sigma^+$, and A $^2\Sigma^+$; LiH, X $^1\Sigma^+$, and A $^1\Sigma^+$; BeH, X $^2\Sigma^+$, and A $^2\Pi$; BH, X $^1\Sigma^+$, and a $^3\Pi$; CH, X $^2\Pi$, and A $^2\Delta$; NH, X $^3\Sigma^-$, and a $^1\Delta$; OH, X $^2\Pi$, and A $^2\Sigma^+$; FH, X $^1\Sigma^+$, and A $^1\Pi$; NeH, X $^2\Sigma^+$, and A $^2\Sigma^+$. The values of R_0 used to generate the coordinates at which the energies were calculated are given in Table 6.

From the study on H_2 in Part 1, it is seen that a large basis set and a high level of treatment of electron correlation are necessary in order to accurately obtain the high-frequency components, whereas it is not necessary to sample at such small intervals in the η coordinate. For the set of 20 potential curves, multireference CI calculations performed by using basis sets of cc-pVQZ and larger for the heavy atom and aug-cc-pV5Z for hydrogen were performed at 512 equally spaced points. This is expected to represent some degree of oversampling, so that any instability would be clearly evident as algebraic convergence at high frequencies. The curve was then padded to 2048 points by using the asymptotic energy obtained at the largest atomic separation distance. The results of these analyses are shown in Figures 10−19. Most systems exhibited some form of convergence instability at some point along the curve with aug-cc-pVQZ on the heavy atom, proving to be more reliable than aug-cc-pV5Z for C through Ne. Where instabilities did occur, as evidenced by algebraic convergence in the Fourier spectrum, in all but one case, the curves were continuous, exhibiting discontinuities in the first or second finite differences.

The Fourier transforms in Figures 10b−19b are seen to have three regions. At low frequencies, the Fourier coefficients are all positive and decay rapidly with a much smaller amplitude oscillatory component superimposed on the decay. For those curves which exhibit algebraic convergence, the oscillatory behavior is clearly visible through the whole of the mid- and high-frequency regions. For the systems exhibiting exponential decay, there is clear evidence of behavior ranging from multiexponential decay of multiple, interfering oscillatory components to simple single-frequency, single-exponential decay in the mid-frequency portion. At high frequency, many of the transformed curves exhibit a mixture of behavior: either a randomly oscillating intensity pattern (characteristic of white noise expected from numerical convergence truncation) or oscillations with an envelope characteristic of algebraic convergence.

The H_2 X $^1\Sigma_g^+$ and b $^3\Sigma_u^+$ potential curves are shown after mapping to the η coordinate in Figure 10 along with the first 500 values of the accompanying Fourier spectra. The properties of the Fourier spectrum of the X $^1\Sigma_g^+$ mapped potential have been discussed at length in the first section of this paper. The first excited state is repulsive in nature with a very shallow potential energy well at distances around 7.8 Å. The Fourier-transformed spectrum of the mapped potential energy curve

TABLE 6: Summary of convergence characteristics.

molecule: state	R_0 (Å)	exponential convergence rate, k decay rate $= e^{-kn}$ (a_n used for analysis)	algebraic convergence rate, s decay rate $= x^s$ ($500 \leq a_n \leq 1500$)
H_2: $X^1\Sigma_g^+$	0.200479569	0.0642 (100−207)	0.134
H_2: $b^3\Sigma_u^+$	0.28595596	0.119 (28−114)	−1.060
HeH:$X^2\Sigma^+$	0.157693	0.036 (80−160)	0.156
HeH:$A^2\Sigma^+$	0.1594669	0.0427 (50−190)	0.0393
LiH: $X^1\Sigma^+$	0.1180439	0.0298 (100−400)	−0.031
LiH: $A^1\Sigma^+$	0.119817339	0.0267 (100−400)	−0.742
BeH:$X^2\Sigma^+$	0.0919627	0.0326 (94−342)	−0.501
BeH:A $^2\Pi$	0.09201183	0.0312 (94−342)	−1.14
BH: $X^1\Sigma^+$	0.073917107	0.0246 (93−151)	−0.884
BH: a $^3\Pi$	0.07382902	0.0327 (100−300)	−0.867
CH: X $^2\Pi$	0.06093221	0.0328 (112−170)	−1.56
CH: A $^2\Delta$	0.060940033	0.0372 (112−171)	−0.854
NH: X $^3\Sigma^-$	0.05118992	0.0382 (120−165)	−2.33
NH: a $^1\Delta$	0.05155405	0.0731 (120−165)	−1.19
OH: X $^2\Pi$	0.043764183		−1.82
OH: $A^2\Sigma^+$	0.04377572		−0.82
FH: $X^1\Sigma^+$	0.037852089	0.0312 (150−250)	−1.04
FH: A $^1\Pi$	0.038045686	0.0313 (150−350)	−0.382
NeH:$X^2\Sigma^+$	0.033332258	0.0378 (174−318)	−0.386
NeH:$A^2\Sigma^+$	0.038045686	0.0569 (150−220)	−1.576

demonstrates a limiting algebraic convergence indicative of a singularity located at 0.5585 Å. The potential curve does indeed exhibit a discontinuous second derivative at this point, of magnitude consistent with the features in the Fourier spectrum. At lower frequency, the convergence behavior is exponential but clearly contains multiple, interfering components. The increased complexity of the decay, as well as the increased rate of exponential decay, implies that there are multiple singularities associated with the excited-state curve and that these singularities are located further away from the real axis than the singularity associated with the ground-state potential. An estimate of the relative imaginary coordinate location of the convergence limiting singularity can be gained from a comparison of the estimated slopes of the exponential portions of the Fourier spectra. This places the location of the limiting singularity for the triplet excited state 1.85 times the imaginary coordinate position of the singlet ground-state singularity.

Although the Fourier spectra for the series of molecules from HeH to NeH exhibit more complex features than that shown by H_2, some general conclusions may be drawn. First, the application of the same inverse hyperbolic mapping and subsequent Fourier analysis leads to identification of resonances in all of the potentials surveyed. The resonances are associated with particular values of the internuclear distances and hence have their origins in the formation of electronic configurations which decay as this distance is varied. The origins of these resonances appear to be associated with resonant modes of the molecule, because it requires extensive MRCI in order to obtain them; that is, they are not associated with a fluctuation of a single electronic configuration term in the MRCI expansion. The mapped spatial forms of the resonances corresponding to the exponential decays also clearly show modulation of the overall Lorentzian envelopes, consistent with a process involving phase-sensitive behavior. There is an obvious similarity in behavior to the Fano absorption line profiles observed in photoionization experiments.[21−23] If the similarity does translate into an analogy, it would seem reasonable to suggest that the dominant component (i.e., the component corresponding to the unmodulated lowest-frequency Fourier coefficients) is responsible for the background phase shift necessary to induce asymmetry in the shapes of the curves of the smaller components.

The exponential decay constants, (with respect to the $n = 4096$ Fourier components) are tabulated in Table 6 for the exponential decay regions. These values are to be regarded as only an estimation of the supremum decay constants, especially in the cases where there is evidence of multiple resonances giving rise to complex interferences in the decay. The algebraic index for the decay in the high-frequency region is also listed in Table 6.

It is possible to filter out the dominant (unmodulated) low-frequency component by truncating the Fourier series and shifting the high frequencies to lower frequencies. By choosing a truncation point that corresponds to a multiple of the central frequencies of one or more of the components and applying an inverse transformation, the original component(s) can be retrieved without loss of the relative phase information. Although this procedure sacrifices the absolute magnitude of each of the components, the central peak position and phase relationship are maintained for the chosen resonance. In practice, this procedure can only be applied for situations where there is a single component or where the locations of the peaks occur at positions which are whole-number multiples of each other. The peak must also have a clearly identifiable center frequency, which can be difficult to ascertain when there are multiple, overlapping components, accompanied by different relative-phase offsets for each component. This phase sensitive behavior and a possible relationship to the structure of the electronic state manifold of the molecule is most clearly visible for the LiH molecule. In the case of LiH, two resonances appear in both the ground and first excited states (Figure 12c). In the transformed coordinate system, the resonance at the largest position is located at a (mapped) coordinate almost exactly twice the value of that of the smallest, and therefore, it becomes possible to preserve the relative phases between the two resonances. Choosing a value for the frequency cutoff in the Fourier spectra of both the ground and excited states so that the low-frequency (all positive) component has been virtually eliminated yields the peaks shown in Figure 12c after shifting and inverse transformation. Evident in the figure is the relative phase shift of approximately π between the two states for both peaks, as well as a relative difference in phase of $\pi/2$ for the two peaks within each state. Accompanying the changes in phase is a reversal of the intensity pattern. The curves associated with figures 10c−19c were obtained by attempting to identify the center position of the largest resonance, filtering and shifting the Fourier spectrum appropriately, and then applying an inverse

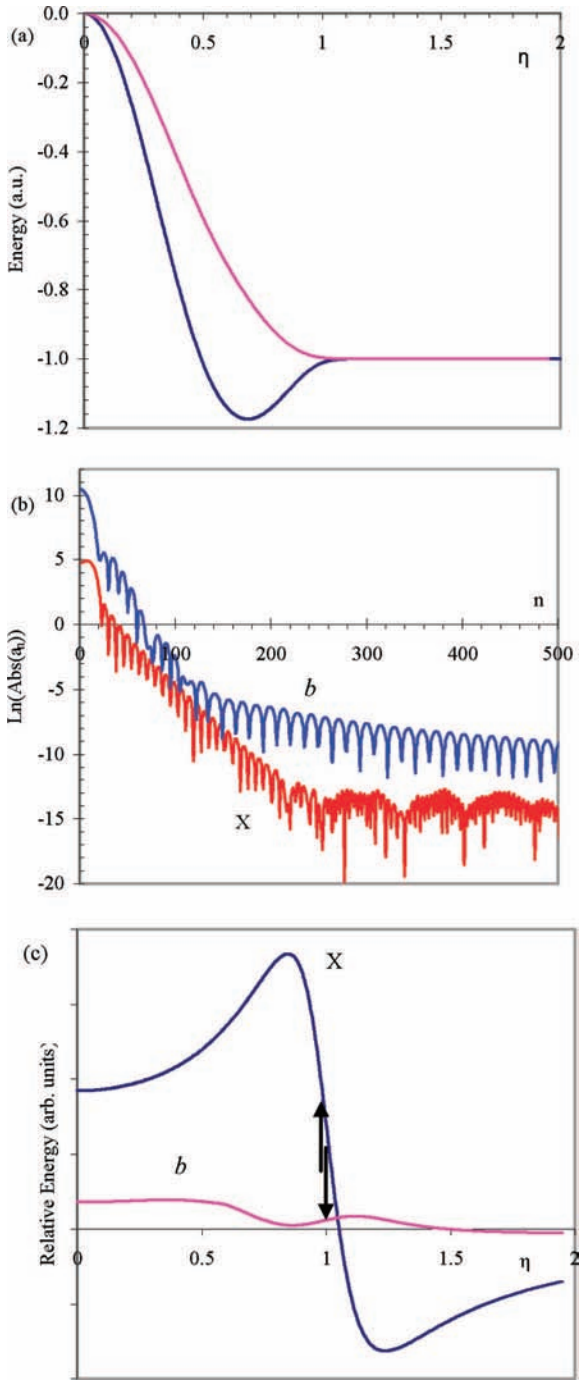

Figure 10. H_2 X $^1\Sigma_g^+$ and b $^3\Sigma_u^+$ MRCI (H: aug-cc-pV5Z). (a) Mapped potential energy curves. (b) Modulus of the $n < 500$ Fourier coefficients. The Fourier coefficients of the b state have been vertically offset by +5 units. (c) Filtered exponential decay region for the H_2X and b states after shifting and inverse Fourier transformation. Arrows indicate regions with correct phase.

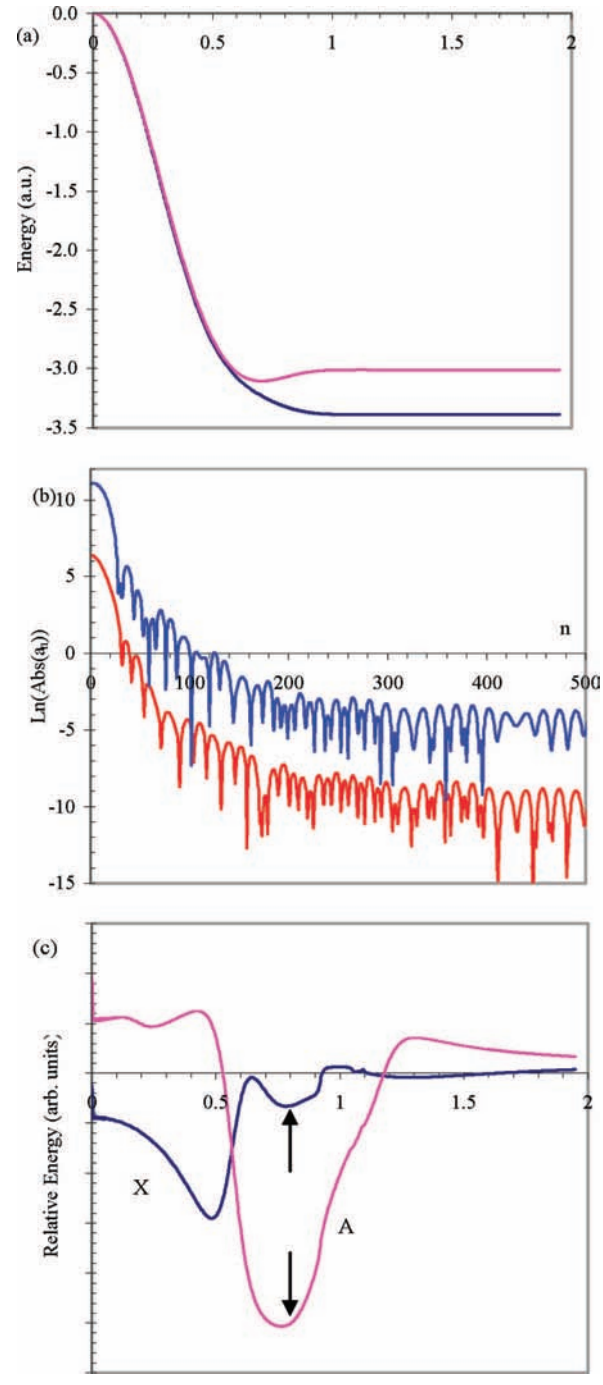

Figure 11. HeH X $^2\Sigma^+$ and A $^2\Sigma^+$ MRCI (H, He: aug-cc-pV5Z). (a) Mapped potential energy curves. (b) Modulus of the $n < 500$ Fourier coefficients. The Fourier coefficients of the A state have been vertically offset by +5 units. (c) Filtered exponential decay region after shifting and inverse Fourier transformation. Arrows indicate regions with correct phase.

Fourier transformation. Any resonance with a center frequency indicated by the arrows in the figures will then appear with the correct phase and shape as in the original potential curve, but the absolute contribution to the energy will not be accurate because this information is lost by shifting the Fourier components. Attempts at extrapolating the exponentially decaying component back indicate that the absolute magnitudes of these resonances are typically 1−2 orders of magnitude less than the primary (nonmodulated) component. In favorable cases, there is evidence of resonances of much smaller magnitude in the filtered curves.

There appears to be relationships within the structures observed in the filtered spectra for some of the molecules chosen. For example, the OH ground state exhibits two resonances which appear to be related by a phase shift of π. The A state also has two resonances related by the same phase shift, but they appear to be inverted with respect to the resonances in the ground state that they are closest to. Additionally, the excited-state curves appear to be shifted symmetrically with respect to the midpoint between the ground-state resonances, suggesting a doublet structure. The absolute magnitudes of the two resonances indicated by arrows in Figure

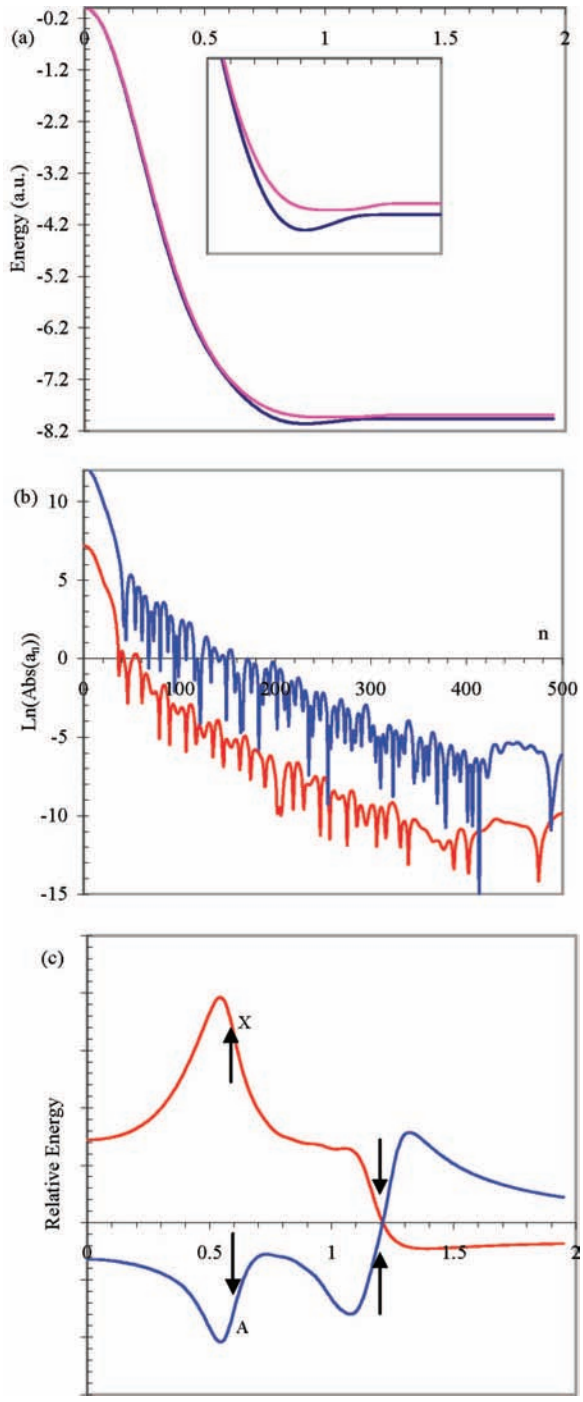

Figure 12. LiH X $^1\Sigma^+$ and A $^1\Sigma^+$ MRCI (H: aug-cc-pV5Z; Li: cc-pV5Z). (a) Mapped potential energy curves. The insert details the bound region for the two states. (b) Modulus of the $n < 500$ Fourier coefficients. The Fourier coefficients of the A state have been vertically offset by +5 units. (c) Filtered exponential decay region after shifting and inverse Fourier transformation. Arrows indicate regions with correct phase.

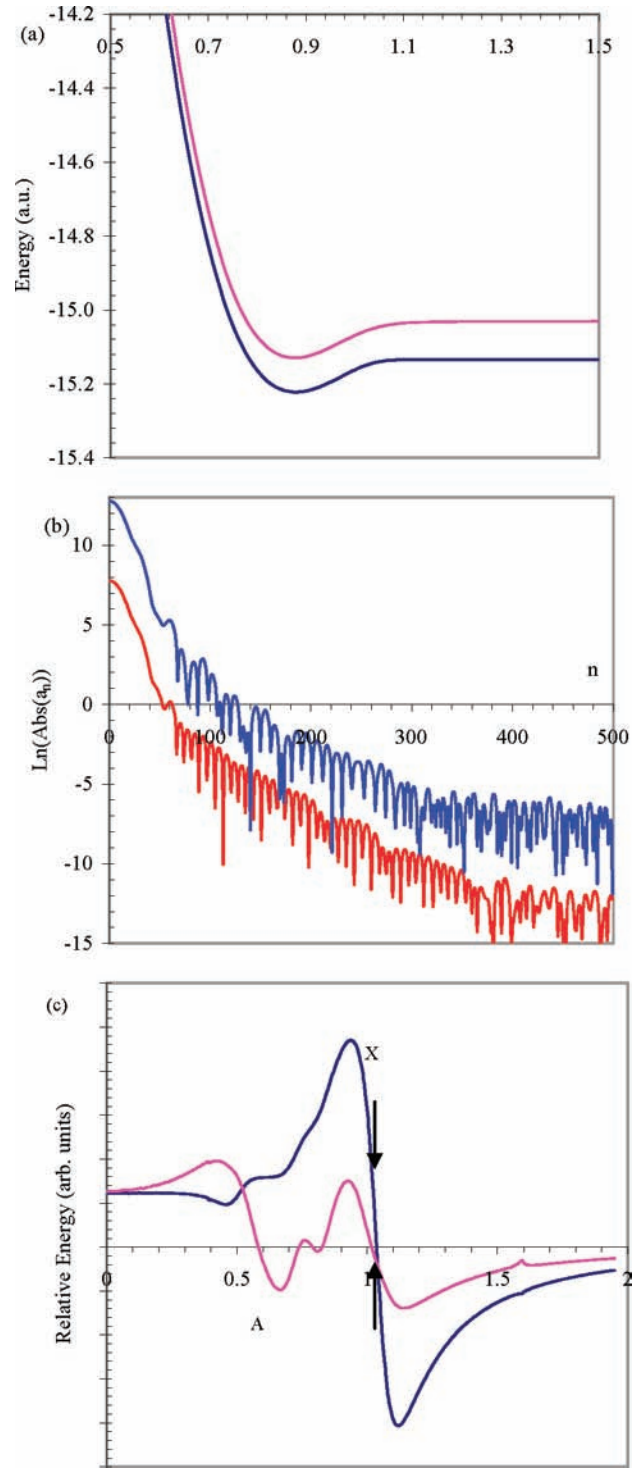

Figure 13. BeH X $^2\Sigma^+$ and A $^2\Pi$ MRCI (H: aug-cc-pV5Z; Be: cc-pV5Z). (a) Mapped potential energy curves (only the regions around the potential minima are shown). (b) Modulus of the $n < 500$ Fourier coefficients. The Fourier coefficients of the A state have been vertically offset by +5 units. (c) Filtered exponential decay region for the BeHX and A states after shifting and inverse Fourier transformation. Arrows indicate regions with correct phase.

17c are 0.133 and 2.46 millihartree for the ground and excited states, respectively. It is possible to directly measure this because in this case, both features are observable as distinct steps in the MRCI potential-energy curves as expected from the algebraic convergence noted for both Fourier spectra.

If, as is postulated here, the resonances correspond to the formation of intermediate states, it suggests that those singularities occurring on the real axis giving rise to algebraic convergence are either extremely narrow (and hence correspond to a singularity lying very close to the real axis, giving rise to very slow convergence in the Fourier spectrum) and the sample spacing between points is too great to accurately measure the shape without introducing a discontinuity (undersampling) or the level of theory used is inadequate (limited basis set, restricted correlation) to correctly determine the spatial dependence of the resonances ending up with a singularity on the real axis.

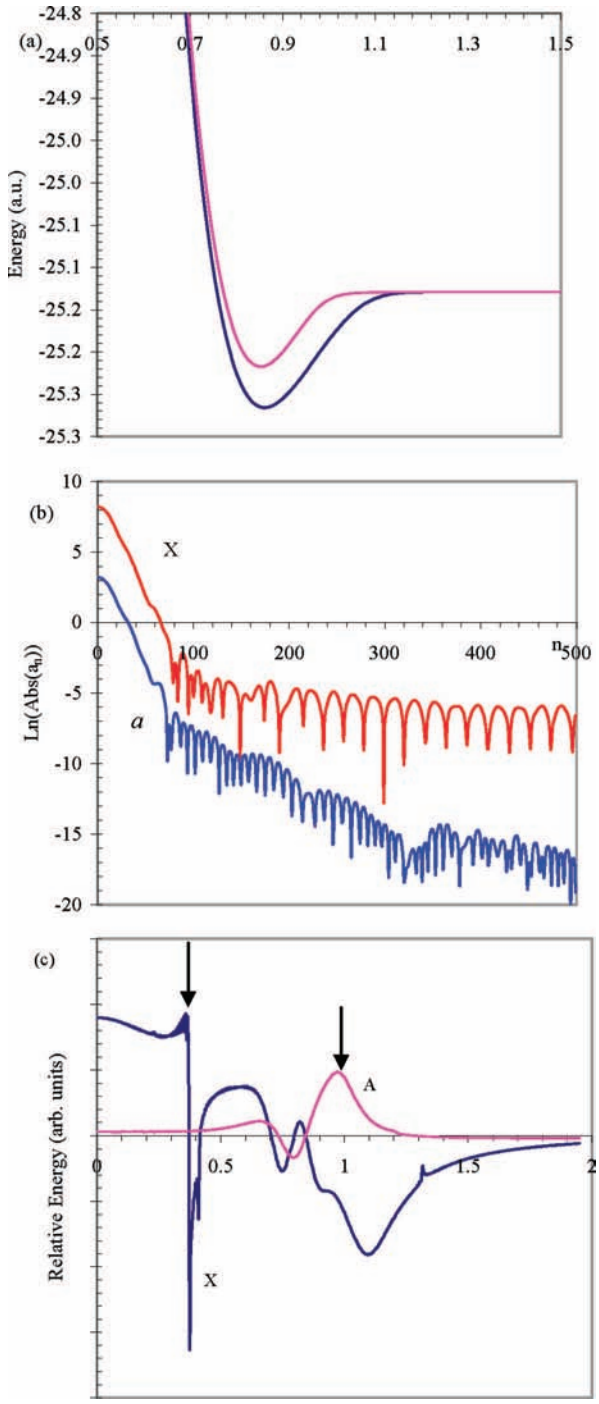

Figure 14. BH X $^1\Sigma^+$and a $^3\Pi$ MRCI (H,B: aug-cc-pV5Z). (a) Mapped potential energy curves (only the regions around the potential minima are shown). (b) The modulus of the $n < 500$ Fourier coefficients. The coefficients for the a state have been vertically offset by -5 units. (c) Filtered exponential decay region after shifting and inverse Fourier transformation. Arrows indicate regions with correct phase.

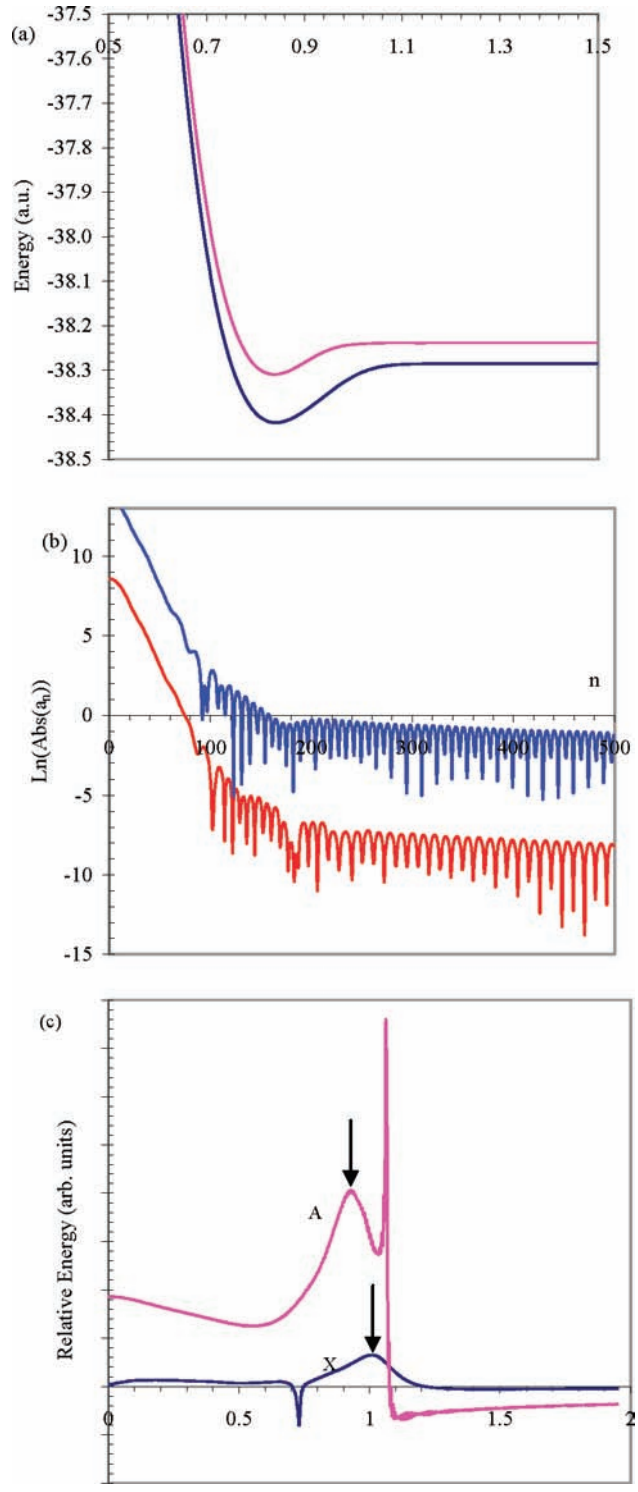

Figure 15. CH X $^2\Pi$, A $^2\Delta$ MRCI (H: aug-cc-pV5Z; C: aug-cc-pVQZ). (a) Mapped potential energy curves (only the regions around the potential minima are shown). (b) Modulus of the $n < 500$ Fourier coefficients. The Fourier coefficients of the A state have been vertically offset by $+5$ units. (c) Filtered exponential decay region after shifting and inverse Fourier transformation. Arrows indicate regions with correct phase.

The notion of a configuration that decays to one or more configurations of greater stability is usually associated with the chemical notion of an intermediate. Intermediates correspond to positions of local potential energy minima located higher in energy than the global minimum on the potential energy curve. In the analysis for the series of molecules HX, above, the resonances that are observed can give rise to quite complicated oscillations in the potential-energy curves, resulting in distortions away from purely Lorentzian components. The intensity of the dominant low-frequency component also masks the individual contributions from each of the minor resonances. At one extreme, the phase is such that the peak appears to have the structure associated with a transition state (positive, distinct maximum); at the other extreme, the phase inverts to give rise to an intermediate state (negative, distinct minimum), and in between, there is quite complex oscillatory behavior as the underlying components interfere.

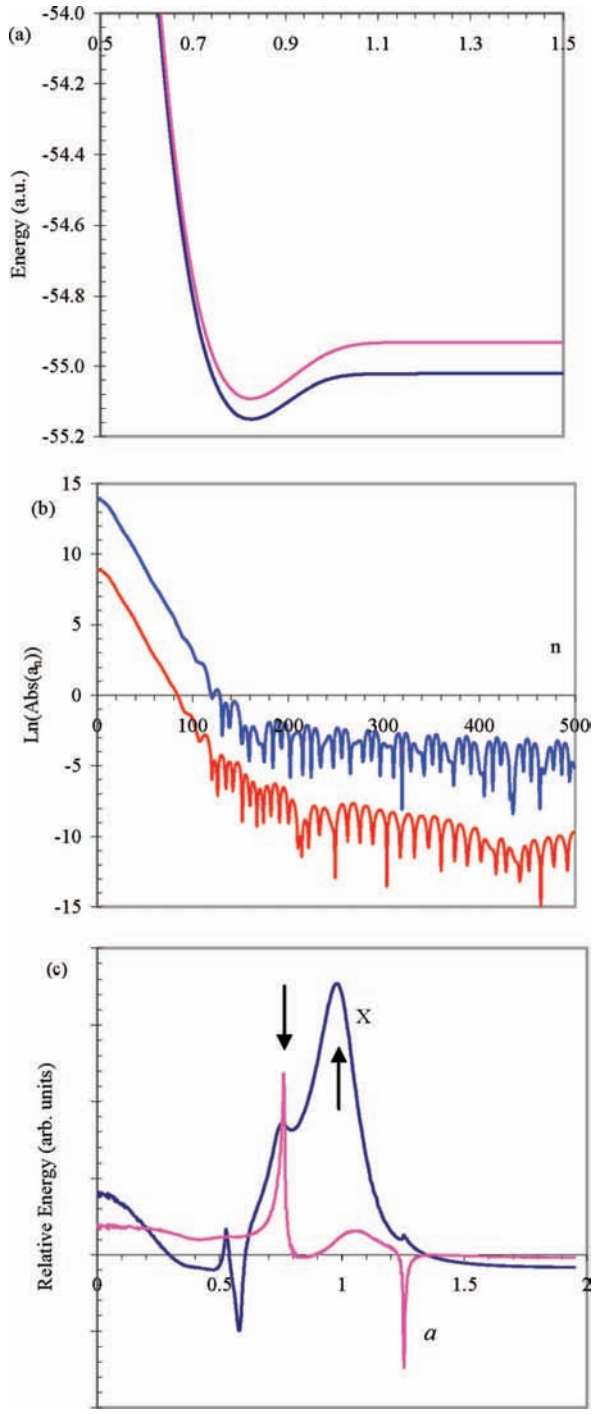

Figure 16. NHX $^3\Sigma^-$, $a\ ^1\Delta$ MRCI (H: aug-cc-pV5Z; N: aug-cc-pVQZ). (a) Mapped potential energy curves (only the regions around the potential minima are shown). (b) Modulus of the $n < 500$ Fourier coefficients. The Fourier coefficients of the a state have been vertically offset by +5 units. (c) Filtered exponential decay region after shifting and inverse Fourier transformation. Arrows indicate regions with correct phase.

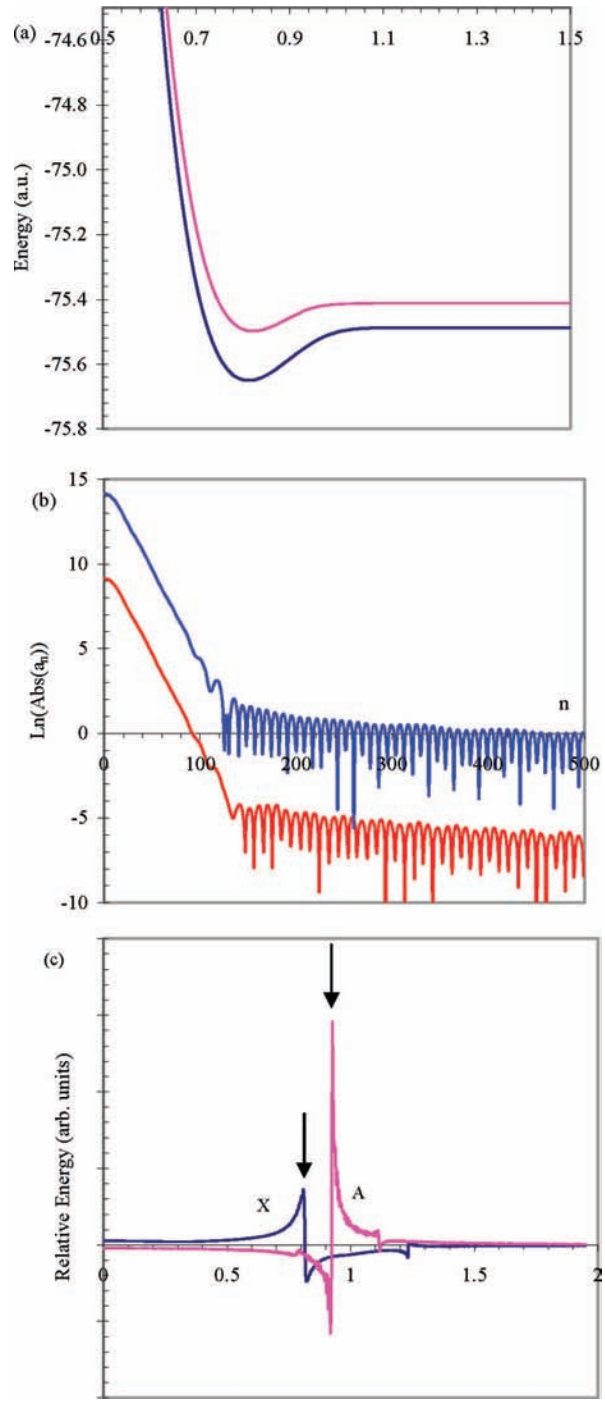

Figure 17. OH X $^2\Pi$ and A $^2\Sigma^+$ MRCI (H: aug-cc-pV5Z; O: aug-cc-pVQZ). (a) Mapped potential energy curves (only the regions around the potential minima are shown). (b) Modulus of the $n < 500$ Fourier coefficients. The Fourier coefficients of the A state have been vertically offset by +5 units. (c) Filtered exponential decay region after shifting and inverse Fourier transformation. Arrows indicate regions with correct phase.

The various components due to the smaller resonances combine in an additive manner with the dominant component to give the overall total potential. For most of the molecules and states surveyed in this work, it is apparent that there are relatively few resonances contributing to the overall sum. Identification of the positions, magnitudes, widths (i.e., decay rates), and background phase offsets of each of the components would give a concise and comprehensive description of the overall potential curve.

Conclusion

After the application of an inverse hyperbolic cosine coordinate transformation, the ab initio potential energy curves of the ground and first excited electronic states of the first 10 diatomic hydrides become amenable to Fourier analysis. The RHF curve for the ground state of hydrogen failed to locate any singularity except for the one corresponding to nonconvergence over the sampling interval employed. The Fourier spectrum of the UHF curve similarly demonstrated algebraic

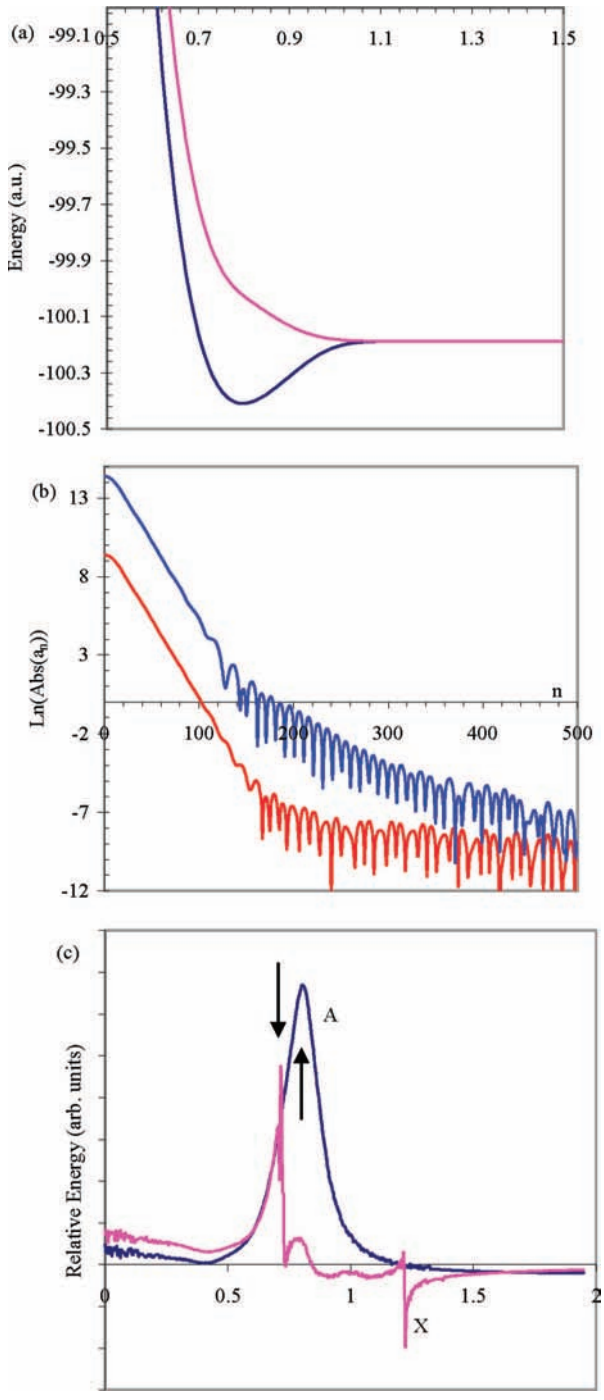

Figure 18. HF X $^1\Sigma^+$and A $^1\Pi$ MRCI (H: aug-cc-pV5Z; F: aug-cc-pVQZ). (a) Mapped potential energy curves (only the regions around the potential minima are shown). (b) Modulus of the $n < 500$ Fourier coefficients. The Fourier coefficients of the A state have been vertically offset by +5 units. (c) Filtered exponential decay region after shifting and inverse Fourier transformation. Arrows indicate regions with correct phase.

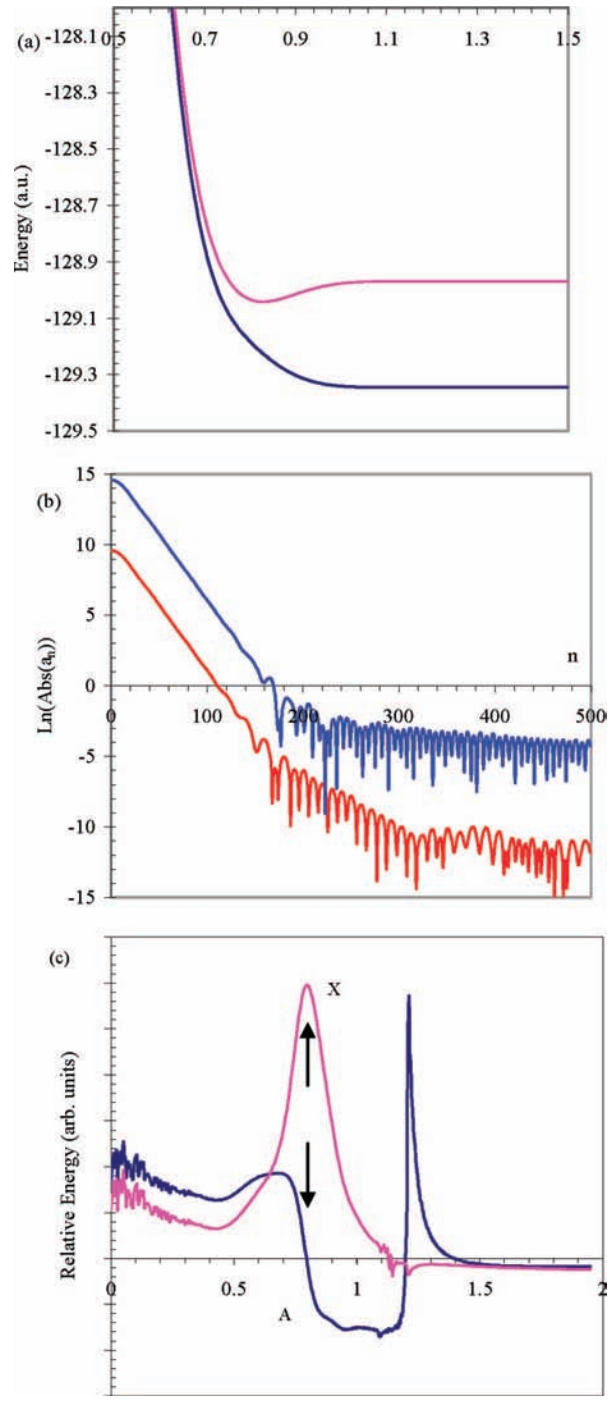

Figure 19. NeH X $^2\Sigma^+$ and A $^2\Sigma^+$ MRCI (H: aug-cc-pV5Z; Ne: aug-cc-pVQZ). (a) Mapped potential energy curves (only the regions around the potential minima are shown). (b) Modulus of the $n < 500$ Fourier coefficients. The Fourier coefficients of the A state have been vertically offset by +5 units; (c) Filtered exponential decay region after shifting and inverse Fourier transform.

convergence because of the location of a singularity along the internuclear coordinate. The Fourier spectra obtained from the potential-energy curves for the ground state of hydrogen calculated at the highest level of theory (full-CI) are compact and decay with exponential convergence, indicating that the limiting singularities are located off the real axis in the complex plane. For the ground and first excited states of the series of molecules HX (X = H−Ne), the limiting convergence was either exponential or algebraic, indicating the presence of singularities located on the complex plane or on the real axis, respectively.

For the cases that exhibit exponential convergence, the magnitude of the random errors in the calculated potential-energy curves can be clearly seen from the noise floor in the Fourier spectrum which can be trivially removed by introducing a high frequency cutoff. The introduction of this cutoff frequency allows for an optimum sampling strategy to be established over the whole of the potential-energy curve. Undersampling of the potential curve has deleterious consequences for the determination of the equilibrium bond length, whereas oversampling gives no further improvement in the

determination of the position of the minimum in the curve. The lowest-frequency Fourier components of the QCISD curves show an empirical N^{-2} dependence (where N is the total number of basis functions used), allowing a straightforward extrapolation to the infinite basis set limit.

From a theoretical perspective, the trends associated with the different levels of theory, especially those associated with increasing the size of the basis set as well as dramatic differences due to inclusion of electron correlation, are clearly evident in the Fourier spectra. Although application of the Fourier transform requires information over the whole of the potential energy curve, as demonstrated by this work, the resulting information that can be extracted from the transformed curve allows definite statements to be made regarding the location of singularities associated with the curves. The general methodology could be expected to have widespread applicability for analysis, sampling, and interpolation of potential energy surfaces including straightforward generalization to multidimensional applications. In particular, the compact nature of the Fourier spectra obtained at the full-CI level indicates that this methodology should be useful for the evaluation of the performance of theoretical methods over the whole of the potential curve and should thus be a complimentary method to comparison with thermochemical data.

In addition to the practical applications described above, the existence of a compact Fourier spectrum obtained following an inverse hyperbolic coordinate transformation is anecdotal evidence that the chemical bond may have hyperbolic character with respect to the internuclear distance. Such an observation is seemingly without precedence in the chemical literature and is not an obvious prediction from existing molecular electronic structure theory. Alternatively, there is no general theorem precluding such a relationship, and it may be possible to recast the existing theory by using an alternative coordinate system, such as the one presented in this work, so that the equations in Fourier space take on a particularly simple form, as the results presented here are suggestive of.

Additionally, it would appear that for accurate potential-energy curves, there are features that are best described by singularities existing in the complex plane. The ability to accurately locate singularities on the complex plane is dependent on the level of theory employed in the calculation, as well as being able to isolate individual resonances from overlapping combinations. The nature of the singularities and their locations are likely to have an underlying fundamental physical significance because such mathematical entities usually arise from resonances in physical theories. The resonances observed here appear to have properties analogous to resonances in scattering theory (i.e., phase and rate of decay are important quantities) and would therefore appear to represent the formation and decay of intermediate electronic configurations as the internuclear distance is varied. As these resonances contribute directly to the value of the total potential, it would appear that an understanding of their origins and lifetimes could contribute directly to understanding the processes of formation and rupture of the chemical bond.

The identification of the underlying resonances required the introduction of the hypothesis that there is an underlying hyperbolic characteristic to the chemical bond. The coordinate mapping via the application of an inverse hyperbolic cosine transformation has been introduced from a heuristic viewpoint and does not have any rigorous a priori theoretical basis. The observation that the resonances for the variety of systems studied here are more or less symmetrical (once the phase shift has been accounted for), independently of the value of their position in the mapped coordinate, suggests that the general transformation used is not grossly in error and should be applicable to a wider range of systems than just those studied here. The facility with which mathematical methods of analysis have been applied to the series of states presented here suggests that there is good reason for pursuing this methodology.

Acknowledgment. Helpful comments from the referee and access to the computing facilities of the Centre of Theoretical Chemistry and Physics of Massey University are gratefully acknowledged.

References and Notes

(1) Bracewell, R. N. *The Fourier Transform and its Applications*, 3rd ed.; McGraw Hill, 2000.
(2) Shannon, C. E. *Bell Sys. Tech. J.* **1948**, *27*, 379.
(3) Shannon, C. E. *Bell Sys. Tech. J.* **1948**, *27*, 623.
(4) Boyd, J. P. *Chebyshev and Fourier Spectral Methods*; Springer-Verlag, 1989.
(5) Subotnik, J. E.; Sodt, A.; Head-Gordon, M. *J. Chem. Phys.* **2005**, *125*, 074116.
(6) Subotnik, J. E.; Sodt, A.; Head-Gordon, M. *J. Chem. Phys.* **2008**, *128*, 034103.
(7) Woon, D. E. *J. Chem. Phys.* **1993**, *98*, 1358.
(8) Kendall, R. A.; Harrison, R. J. *J. Chem. Phys.* **1992**, *96*, 6796.
(9) Dunning, T. H., Jr *J. Chem. Phys.* **1989**, *90*, 1007.
(10) Peterson, K. A.; Woon, D. E. *J. Chem. Phys.* **1994**, *100*, 7410.
(11) Dunning, T. H. *J. Phys. Chem.* **2000**, *104*, 9062.
(12) Frisch, M. J.; Trucks, G. W.; Schlegel, H. B.; Scuseria, G. E.; Robb, M. A.; Cheeseman, J. R.; Zakrzewski, V. G.; Montgomery, J. A., Jr.; Stratmann, R. E.; Burant, J. C.; Dapprich, S.; Millam, J. M.; Daniels, A. D.; Kudin, K. N.; Strain, M. C.; Farkas, O.; Tomasi, J.; Barone, V.; Mennucci, B.; Cossi, M.; Adamo, C.; Jaramillo, J.; Cammi, R.; Pomelli, C.; Ochterski, J.; Petersson, G. A.; Ayala, P. Y.; Morokuma, K.; Malick, D. K.; Rabuck, A. D.; Raghavachari, K.; Foresman, J. B.; Ortiz, J. V.; Cui, Q.; Baboul, A. G.; Clifford, S.; Cioslowski, J.; Stefanov, B. B.; Liu, G.; Liashenko, A.; Piskorz, P.; Komaromi, I.; Gomperts, R.; Martin, R. L.; Fox, D. J.; Keith, T.; Al-Laham, M. A.; Peng, C. Y.; Nanayakkara, A.; Challacombe, M.; Gill, P. M. W.; Johnson, B.; Chen, W.; Wong, M. W.; Andres, J. L.; Gonzalez, C.; Head-Gordon, M.; Replogle, E. S.; Pople, J. A. *Gaussian 98*, Development Version, revision A.11.4; Gaussian, Inc.: Pittsburgh, PA, 1998.
(13) Werner, H.-J.; Knowles, P. J.; Lindh, R.; Manby, F. R.; Schütz, M.; Celani, P.; Korona, T.; Rauhut, G.; Amos, R. D.; Bernhardsson, A.; Berning, A.; Cooper, D. L.; Deegan, M. J. O.; Dobbyn, A. J.; Eckert, F.; Hampel, C.; Hetzer, G.; Lloyd, A. W.; McNicholas, S. J.; Meyer, W.; Mura, M. E. ; Nicklass, A.; Palmieri, P.; Pitzer, R.; Schumann, U.; Stoll, H.; Stone, A. J.; Tarroni, R.; Thorsteinsson, T. *MOLPRO version 2006 1, a package of ab initio programs*; http://www.molpro.net.
(14) Werner, H.-J.; Knowles, P. J. *J. Chem. Phys.* **1988**, *89*, 5803.
(15) Knowles, P. J.; Werner, H.-J. *Chem. Phys. Lett.* **1988**, *145*, 514.
(16) Werner, H.-J.; Knowles, P. J. *J. Chem. Phys.* **1985**, *82*, 5053.
(17) Knowles, P. J.; Werner, H.-J. *Chem. Phys. Lett.* **1985**, *115*, 259.
(18) Kolos, W. *J. Chem. Phys.* **1994**, *101*, 1330.
(19) Huber, K. P.; Herzberg, G. Constants of Diatomic Molecules, data prepared by Gallagher, J.W.; Johnson, R.D., III. In *NIST Chemistry WebBook, NIST Standard Reference Database Number 69*; Linstrom, P. J., Mallard, W. G., Eds.; National Institute of Standards and Technology: Gaithersburg MD, June 2005; http://webbook.nist.gov.
(20) Yang, C-L.; Huang, Y-J.; Zhang, X.; Han, K-L. *J. Mol. Struct. (Theochem)* **2003**, *625*, 289.
(21) Fano, U. *Phys. Rev.* **1961**, *124*, 1866.
(22) Fano, U.; Cooper, J. W. *Phys. Rev.* **1965**, *137A*, 1364.
(23) Fano, U.; Cooper, J. W. *Rev. Mod. Phys.* **1968**, *40*, 441.

JP804945Z